Corrosion Science 238 (2024) 112361

Contents lists available at ScienceDirect

Corrosion Science

journal homepage: www.elsevier.com/locate/corsci

Investigation of in-situ ion release and surface film formation of hcp Mg-Li thin films

Lisa Hanke [a], Lukas Kalchgruber [b], Ulrike Westernströer [c], Dieter Garbe-Schönberg [c], Eckhard Quandt [a], Markus Valtiner [b,*]

[a] Inorganic Functional Materials, Institute for Materials Science, Kiel University, Kiel, Germany
[b] Applied Interface Physics, Institute of Applied Physics, Vienna University of Technology, Vienna, Austria
[c] Marine Climate Research, Institute of Geosciences, Kiel University, Kiel, Germany

ARTICLE INFO

Keywords:
A Magnesium
A Sputtered films
B ICP- MS
B XPS
C Surface films

ABSTRACT

In this work, the dissolution process of magnetron sputtered Mg-Li thin films was investigated by in-situ flow cell/ICP-MS measurements and ex-situ ICP-MS measurements after longer immersion and additional XPS measurements. High Li concentrations are released due to a Li rich carbonate layer formed in air. The depletion of Li leads to preferred Mg release before preferred Li release occurs due to the higher activity of Li and incorporation of Mg in corrosion products. This data provides a baseline for developing release profiles for medical application, more generally, it unravels details of the corrosion mechanism of lightweight MgLi alloys.

1. Introduction

Biodegradable materials such as magnesium (Mg) are of interest for several medical applications to reduce permanent implants' side effects, improve bone healing or release bioactive components [1–4]. A key point of interest is the understanding and control of the degradation rate of such implant materials to verify the lifetime of the implants, avoid adverse effects from fast corroding materials and allow for the adjustment of the material properties to facilitate a better treatment [5–7]. Understanding the degradation process becomes even more crucial if the degradation products, e.g., corrosion products and pH change [4] or ion release [8], are used as therapeutically active species. A material of interest for ion release studies is magnesium-lithium. While the release of lithium (Li) from different materials is already studied [9–12], it was recently proposed to use Mg-Li thin films as a reservoir implant releasing Li for the local treatment for neurological applications [8,13] such as the treatment of bipolar disorder, Alzheimer's or Parkinson's disease [14–17]. The therapy with Li is associated with several side effects and has a small therapeutic window [15,18]. Thus, the control of the concentration is of high importance. Mg can be used as the base material for implants not only because it is already widely studied as a biodegradable and biocompatible material and used in clinical trials and medical applications [2,19] but also because it shows possible positive therapeutic effects [19,20]. The treatment with Mg-based materials is already established for particles loaded with additional drugs or using the degradation products, such as hydrogen. Here, both the benefit of a biodegradable carrier and the effect of Mg itself are taken advantage of [21–24].

Mg-Li alloys can be differentiated in α-Mg-Li, α+β-Mg-Li and β-Mg-Li with α as the hexagonal closed packed (hcp) Mg-rich phase and β as the body centred cubic (bcc) Li-rich phase. Generally, the highest corrosion rate is found in the mixed phase α+β due to the microgalvanic coupling of those phases, while single phases show a lower corrosion rate [25,26]. For hcp α-phase Mg-Li with low Li content, the corrosion process is discussed to be similar to pure Mg with the formation of oxide and hydroxide layers [27,28] and filiform corrosion occurring [26,29]. Li carbonate containing protective layers were also found for Mg-5Li-1Al samples in the hcp phase [30]. For neurological applications, implants need to be produced in small sizes. The properties of such thin films are highly affected by surface effects and can differ from bulk material [31,32]. As previously shown [8], similar to bulk material, Mg-Li thin films with low Li fraction show a corrosion rate similar to Mg thin films in a medium chosen to simulate physiological conditions, while the corrosion rate increases for higher Li fractions.

The ion release of Mg-Li-Zn alloys [33] and Mg-Li-(Al)-(RE) [34] was tested to identify the corrosion rate and influence on cells after longer immersion time for applications as stent material. Zhou et al. found an increase in both Li and Mg release for Mg-8.5 wt% Li in comparison to

* Corresponding author.
E-mail address: markus.valtiner@tuwien.ac.at (M. Valtiner).

https://doi.org/10.1016/j.corsci.2024.112361
Received 13 May 2024; Received in revised form 29 July 2024; Accepted 8 August 2024
Available online 13 August 2024

Mg-3.5 wt% Li [34]. The released Mg and Li concentration from Mg-Li thin films with 1.6 wt% and 9.5 wt% Li in Dulbecco's modified Eagle's medium also showed an increased release of Li and Mg with increasing Li content due to a higher corrosion rate [13]. The in-situ measurement of ion release can give further insights not only into the element concentration available after release but also into the corrosion process itself. Based on the concept of AESEC (atomic emission spectroelectrochemistry) [35–37], combinations of flow cells and inductively coupled plasma – optical emission spectrometry (ICP-OES) or inductively coupled plasma - mass spectrometry (ICP-MS) have been used to analyse Mg and Mg-Li corrosion. In addition to identifying the change in ion release by changing pH, contaminations or determining the stoichiometry of participating ions [38–41], the formation of surface films can also be studied by these techniques. Studies were carried out on β-Mg-Li based alloys to determine the passivation layer formed by analysing the released ion concentration of each element dependent on the applied voltage or after scratching to increase the corrosion rate of those alloys and determines the layer formation before and during immersion [42–44]. By identifying the change in ratio of released Mg and Li, the formation of Li_2CO_3 or MgO doped with Li was proposed.

While the formation of surface films and the ion release have been analysed by surface measurements and in-situ studies for films with higher Li content, for α-Mg-Li, Mg-like corrosion has mainly been assumed, and the influence of Li during the process is often overlooked. Thus, this study aims to gain insight into the process of surface film formation before and during the corrosion of α-Mg-Li in simulated physiological medium, especially for magnetron-sputtered thin films. Since the films with lower Li content proved to be biocompatible and released a concentration in the therapeutic window during the previous study by Bhat et al. [13], a detailed understanding by in-situ studies of films with low Li fraction is also important for the application.

The start of immersion was analysed by online ICP-MS. The addition of an electrochemical set-up in the flow cell allowed the further studying if non-equilibrium conditions are applied to enhance the corrosion rate and identify passivation. The surface composition is determined for further analysis of the surface on as prepared samples and after corrosion. Additionally, 3-day immersion studies were carried out in a medium chosen to simulate physiological conditions, and the released ion concentration was identified after solution extraction to provide information regarding the ion concentration over longer immersion times. Thus, by combining both techniques, the degradation process over different time scales can be described and the profile of ion release for possible treatments can be determined.

2. Material and methods

2.1. Film preparation

Thin films of Mg-Li alloys were fabricated in a Von Ardenne CS730S cluster machine from targets (FHR Anlagenbau GmbH) with Li content of 2.5 wt%, 5 wt% and 9 wt% by magnetron sputtering. A base chamber pressure of $<5*10^{-7}$ mbar, a gas flow of 25 sccm Ar and pressures ($2.3–3.3*10^{-3}$ mbar) adjusted to fabricate samples with low film stress were chosen. As the substrate, 1.5 cm×1.5 cm and 1 cm×1 cm Si chips with additional Al/AlN layers were used. The Al/AlN was added to ensure the same film growth as for the preparation of freestanding thin films for which the AlN is necessary as a sacrificial layer. The Li weight fraction in the prepared films with a thickness of 20 μm (±10 %) resulted in 1.6 wt% (1.60±0.06 wt%), 3 wt% (3.07±0.12 wt%) and 5.5 wt% (5.15±0.69 wt%) of Li [8]. Thus, two sample types (Mg-1.6Li, Mg-3Li) with a hcp α-MgLi phase and one sample type (Mg-5.5Li) with mixed α-MgLi, β-MgLi and Li_2CO_3 were prepared [8].

To study the degradation of the thin films over longer immersion times, freestanding thin films with the same compositions were prepared by UV-lithography, sacrificial layers of AlN and the magnetron sputtering of the Mg-Li alloys. For further information regarding the preparation method see Haffner et al. [45].

2.2. In-situ study

A set-up combining a flow cell and an ICP-MS (inductively coupled plasma - mass spectrometer, Agilent 7900 ICP-MS, Agilent Technologies) was used to measure the ion release from Mg-Li thin films in-situ. The set-up and flow cell were previously described in detail [46]. A flow cell with a three-electrode set-up with an Ag/AgCl reference electrode (RE) and a Pt counter electrode was connected to a Biologic VSP-300 potentiostat. The sample size in contact with solution was determined by the O-ring size of the flow cell with a diameter of 3 mm. 15 mmol HBSS (Hanks' balanced salts H1387, Sigma-Aldrich with added sodium bicarbonate (0.35 g/L), solution diluted with distilled water from 155 mmol) was used and pumped through the flow cell by pressurised nitrogen. A Ga standard was added after the flow cell as a control. The composition of the solution was measured using an ICP-MS. The Mg and Li concentrations were calibrated with a multi-element calibration standard 2a (Agilent) and ICP multi-element standard solution XVI. The overall flow speed of the solution was determined by measuring the overall volume of the solution collected in a flask after the ICP-MS at the end of each measurement. Changes in the flow speed during the measurement could be corrected using signals of other elements included in the solution, but not in the sample, such as Ca.

By considering the exposed area (determined by the O-ring size), the dissolution rate j_m is then defined as the dissolved mass of the specific element per time and area. The dissolution current density was calculated by $i = j_m \cdot z \cdot F/M$ with the molar mass M, Faraday constant F and z the valence number of the ions.

The flow cell was connected in parallel to a direct tube of the solution to the ICP-MS and the measurements were started with the measurement of pure solution before switching to the flow cell to analyse the ion release beginning at the start of the degradation. The first degradation is shown at the time t=0 s. Since the signal is often noisy, additional to the raw data, a smoothed signal is shown additionally in plots to identify the general trend.

The first tests were carried out without applying an additional potential (at open circuit potential, E_{OCV}) for 50–60 min. The E_{OCV} was monitored using the potentiostat. To analyse the degradation further, additional samples were held at fixed voltages (Fig. 1a) of +0.2 V vs. E_{OCV}, −0.9 V vs. Ag/AgCl and −0.5 V vs. E_{OCV} for 15 min (constant voltage, CV) after 10 min of immersion (OCV). Additionally, linear sweeps of voltage (LSV) were applied from E_{OCV} to −0.5 V vs. Ag/AgCl

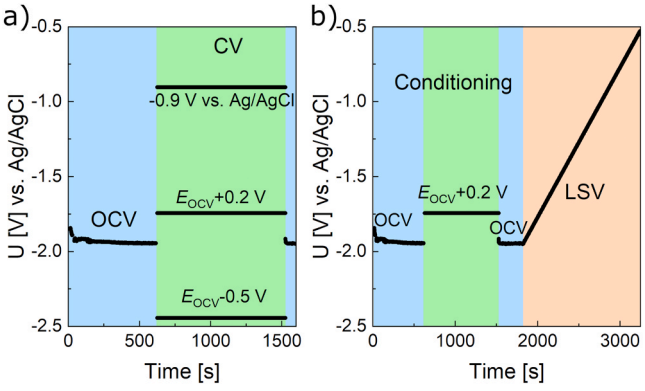

Fig. 1. Exemplary voltage profile applied and measured at flow cell during in-situ ICP-MS measurements: a) For constant voltage (CV) measurements, one of three different potentials is applied after 10 min of open circuit potential measurements (OCV). b) For linear scan voltammetry (LSV) measurements, after OCV, CV at E_{OCV}+0.2 V for 15 min and a further 5 min of OCV for conditioning, the voltage is continuously increased from E_{OCV} up to −0.5 V vs. Ag/AgCl reference electrode.

with a sweep speed of 1 mV/s after 10 min E_{OCV}, 15 min +0.2 V vs. E_{OCV} and 5 min E_{OCV} (see Fig. 1b) for stabilisation.

2.3. 3-day immersion

Freestanding thin films of three Mg-Li alloys were placed in beakers with 100 mL of 155 mmol Hanks' balanced salt solution (HBSS, Hanks' balanced salts H1387, Sigma-Aldrich with added sodium bicarbonate (0.35 g/L)) at a pH of 7.4±0.2 (continuous measurement using a pH meter and adjusted by CO_2 influx) and a temperature of 37±1 °C. After 1 h, 4 h, 24 h and 72 h, 15 mL of solution were extracted, and 15 mL of HBSS from the same starting solution were added. The maximum immersion time was chosen due to the fast degradation for samples with low thickness with both sides exposed to the solution and formation of holes for longer immersion times. The extracted solution was then diluted with ultra-pure DI water (MilliQ, QPod Element) at a dilution factor (DF) of 10 for the measurement of Li and Fe, and DF 2000 for the measurement of Mg for high-resolution inductively coupled plasma - mass spectrometry (HR-ICP-MS, Element XR, Thermo Fisher Scientific) as described in [8]. The Mg and Li concentrations of the blank solution and after corrosion at each time point were determined. The solution partially evaporated over the measurement time. Thus, a beaker with a blank solution was heated simultaneously in a similar set-up to assess the evaporation over the measurement duration. The data from the measurement was used to calculate the released masses (measured concentration and calculations described in supplementary).

2.4. Surface composition characterisation

Four samples per alloy type were used to analyse the sample's surface composition before corrosion, after contact with the solution and after corrosion. One sample was measured as prepared, one was dipped into HBSS (155 mmol) shortly before measurement, and two samples were corroded for 1 h in HBSS. For the two corroded samples, one is stored in air and one in ethanol between corrosion and measurement. All samples were analysed using X-ray photoelectron spectroscopy (XPS) measurements. An Axis Supra spectrometer from Kratos Analytical at the Ceitec Nano Research Infrastructure was utilised. An aluminium anode that produced Al Kα X-rays was used as a radiation source. Since the samples have low conductivity on the surface due to oxide formation and, thus, can show a peak shift due to charging effects, they were measured with charge neutralisation. The samples were mounted on copper tape. The data was evaluated using the software CasaXPS (Version 2.3.23PR1.0). After subtracting a Shirley-type background, the binding energy scale was calibrated by shifting the C 1 s main peak to 284.8 eV.

3. Results

3.1. In-situ ion release at the start of immersion

The ion release of two hcp Mg-Li thin films with Li fractions of 1.6 wt % and 3 wt% were measured in-situ in 15 mmol HBSS by placing samples in a flow cell directly connected to an ICP-MS. In addition to the two hcp Mg-Li alloys, Mg-5.5Li films with very low content of the additional β-phase [9] were analysed for comparison to a mixed-phase material with a higher corrosion rate.

For the first tests, no voltage was applied. Fig. 2 shows the release of Mg and Li directly after contact with the solution exemplarily for one sample per alloy. For all samples, a high release of Li directly after contact is detected, while no such peak can be found in the Mg release. The peak shows a very sharp increase and decrease. This behaviour can be explained by a Li-rich, easily soluble layer on the surface. The distribution of ions in the solution during transport to the ICP-MS might influence the peak width and, therefore, it might be broader than the actual released profile [36]. The height of the peak in the dissolution current density of Li i_{max} increases with increasing Li fraction in the film (Fig. 2b). This height can be influenced by the Li fraction at the surface due to, e.g., a thicker or more complete layer of a Li-rich component and the rate of degradation.

Fig. 2b shows the current density of Mg and Li ions after the direct contact at an immersion time of 3000 s (average of values between 2800 s and 3200 s, $i_{0,Mg}$, $i_{0,Li}$). Mg and Li release increase with increasing Li fraction, showing a higher corrosion rate. The ratio of released Mg and Li ions can be determined to identify not only the change in rate but also changes in the degradation process and the Li release. It is given in

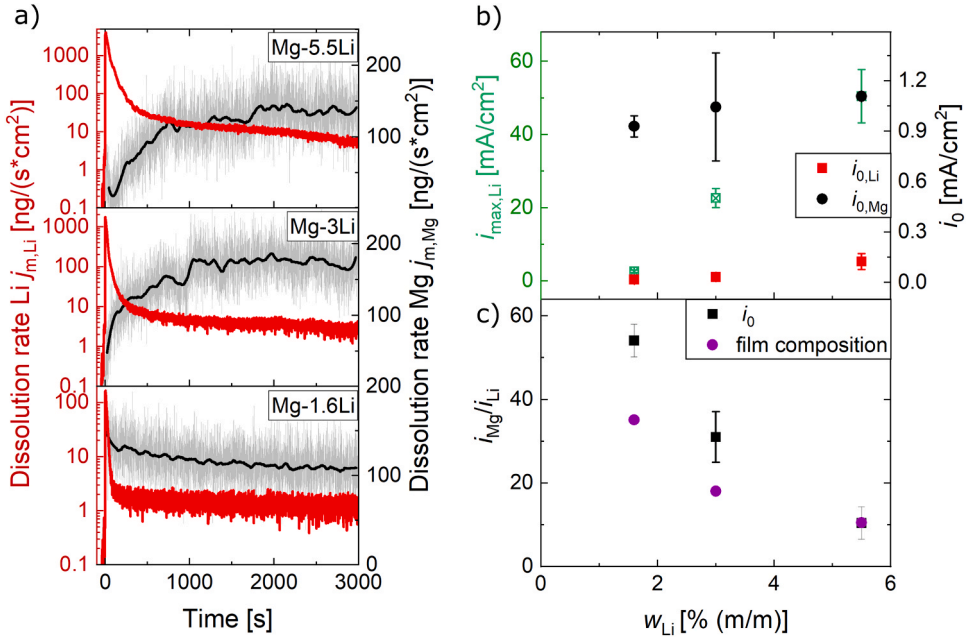

Fig. 2. Ion release of Mg-Li alloys at E_{OCV}. a) Dissolution rate j_m of Mg and Li over 3000 s starting at the contact of the sample with 15 mmol HBSS. For better visualisation of both the peak at the start and the later release, the rate for Li is plotted logarithmically. b) Height of peak at the beginning of Li release ($i_{max,Li}$) and dissolution current density of Mg and Li after 3000 s ($i_{0,Li}$, $i_{0,Mg}$). c) Calculated ratio of $i_{0,Mg}/i_{0,Li}$ (see b) and ratio calculated from the composition of the entire film.

Fig. 2c, additional to the ratio available in the bulk of the film itself determined from the average composition in the overall alloy thin film. For Mg-1.6Li, a higher Mg fraction is released. The difference to the bulk values then shrinks until a ratio similar to bulk is found for Mg-5.5Li. Thus, a preferred release of Mg or a depletion of Li in the layer under the direct (Li-rich) surface can be assumed for Mg-Li with low Li content. It has to be noted that this ratio is determined after relatively short times and, therefore, does not give information about the release from the bulk of the thin film after longer immersion times.

In Fig. 3, the Mg:Li ratio over the 50 min of immersion is shown for Mg-1.6Li and Mg-3Li to identify the influence of time. The time resolved analysis can give further insight into a possible formation of passivation or a change of surface to bulk. After the first peak of Li release, a ratio higher than in the film is directly present and relatively stable or slightly increasing for Mg-1.6Li, while an increase in the ratio is measured for Mg-3Li. The slower and ongoing increase could be influenced by a longer influence of a likely Li-rich layer (as determined by the Li peak measured at the beginning) for Mg-3Li before a higher Mg release is reached, either due to depletion of Li or the preferred release of Mg. The steady state as observed for Mg-1.6Li is not found for Mg-3Li during the first 50 min of immersion.

The E_{OCV} measured during these experiments determined after 2000 s- 3000 s of immersion decreases from −1.71 ± 0.07 V for Mg-1.6Li to −1.86 ± 0.01 V for Mg-3Li. Since Li has a lower electrode potential than Mg, it is expected that the overall potential of the MgLi alloy is reduced with increasing Li content.

Fig. 4 shows the ion release under anodic and cathodic polarisation and, therefore, under an either enhanced (+0.2 V vs. E_{OCV}) or suppressed (-0.5 V vs. E_{OCV}) degradation. The potentials were applied for 15 min after immersion at E_{OCV} for stabilisation (see Fig. 1a). Additionally, samples were held at −0.9 V vs. Ag/AgCl (anodic polarisation) since previous studies on β-Mg-Li found a change in composition and, thus, dissolution of a passivating layer above −1.05 V vs. Ag/AgCl [43]. The current measured by the flow cell decreases to around −0.009 mA at −0.5 V vs. E_{OCV} and increases to about 0.01 mA at +0.2 V vs. E_{OCV} and to 0.02–0.03 mA at −0.9 V vs. Ag/AgCl for both sample types (supplementary figure 1). For Mg-3Li, a continuous further decrease/increase is determined during the application of the constant voltage. In Fig. 4, a step-like increase in both Mg and Li release for an anodic polarisation is found with the highest increase in dissolution rate at −0.9 V vs. Ag/AgCl due to the enhanced dissolution kinetics. For Mg release, both anodic polarisations lead to similar dissolution rate changes. While the Mg signal is nearly completely suppressed at cathodic polarisation, especially for Mg-3Li, no identifiable step and a continuing release of Li is measured. This can be affected by the lower electrode potential of Li and the continuing influence of the first strong release peak. The ratio of dissolution current density of Mg:Li for an enhanced potential increases, thus indicating an increased Mg release, especially for −0.9 V vs. Ag/AgCl (supplementary table 2).

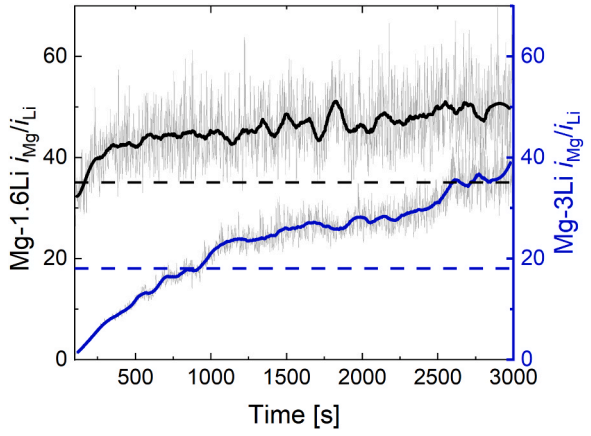

Fig. 3. Ratio of dissolution current density of Mg and Li i_{Mg}/i_{Li} for Mg-1.6Li and Mg-3Li at E_{OCV} over 3000 s. Due to the high release of Li at the beginning, the ratio is shown starting at 100 s. The ratio in the bulk, calculated from the composition of the alloy, is given by dashed lines.

A continuous voltage increase from E_{OCV} to −0.5 V vs. Ag/AgCl is performed on all sample types (LSV). For conditioning, the samples are previously held at a voltage of +0.2 V vs. E_{OCV} for 15 min (Fig. 1b) to enhance the corrosion and, therefore, the formation of corrosion products and passivation layers. Fig. 5a shows the electrical current density measured for one sample per type. For all types, a region of passivation can be found. Exemplary release rate curves vs. the applied voltage are given in Fig. 5b (data sets of 2 samples per type vs. time can be found in supplementary figure 2). In general, the release increases with enhanced voltage. Additionally, a plateau or a change in release around a potential of −1.25 V to −0.75 V occurs before the ion release further increases. For Mg-1.6Li and Mg-3Li, a stabilisation or even decrease of release of both Mg and Li occurs. While the release increase starts again at around -0.75 V for Mg-1.6Li, for Mg-3Li, an additional drop or change in slope is visible around this voltage. Mg-5.5Li only shows short continuous release before the dissolution rate increases with a similar slope as before the passivation region. The difference in the release profiles is even more visible when comparing the ratio of i_{Mg}/i_{Li} (Fig. 5c). The ratio increases slightly for Mg-1.6Li from around −1.2 V and shows a sharp increase and decrease around the threshold voltage for Mg-3Li. A continuous increase over the whole measurement is shown for Mg-5.5Li. Thus, even though a change in the release profile of the individual ions occurs for the mixed-phase material, this does not affect the released ratio in the passivation region specifically. The composition of a passivating layer does not differ from the ratio in the thin film for the material with a second phase. For pure hcp, in both cases, a shift to more Mg release can be found, even though the ratio is already higher than present in the bulk material. A short increase in the ratio for Mg-3Li could hint at a higher concentration of Mg in the surface film but no increased availability for corrosion, while Mg-1.6Li shows a preferred release of Mg even of the material itself after reaching −1 V.

3.2. Release over 3 days

The release of Mg and Li of the three different types of Mg-Li thin films during an immersion time of 3 days in HBSS at a pH of 7.4 and a temperature of 37 °C is analysed by ICP-MS measurements on extracted solution. Fig. 6a and 6b show the dissolved Li and Mg mass (overall released mass until the point of measurement) and the dissolved mass normalised with the element mass available in the as-prepared film.

A higher Li fraction in the film leads to more Li mass released. The Li content of Mg-1.6Li and Mg-3Li is continuously dissolved, and when the Li content of the samples itself is taken into account, no significant difference is determined. Thus, the release in Li is proportional to the Li amount in the film for those samples. The Li release slows down after longer immersion times, hinting at a possible decrease in corrosion rate or passivation over time. For Mg-5.5Li, a much higher release and higher deviation of measured ion masses can be determined compared to the other alloys.

The Mg release in Fig. 6b does not show substantial differences between the alloys. Since Mg is the main component in the weight of all alloys, dividing by the mass in the film also does not significantly influence the results. While after immersion times of up to 24 h, Mg-1.6Li and Mg-3Li show similar release, the release after 72 h for Mg-3Li is lower. However, the data for Mg-3Li after 72 h also shows the highest standard deviation. In Fig. 6c, the fraction of released Mg in comparison to Li mass is given for further insight into the ion release process. Additionally, the calculated fractions are marked by dashed lines for each alloy. For both Mg-1.6Li and Mg-3Li, the ratio decreases during immersion, with Mg-1.6Li samples having a higher Mg fraction after 1 h than present in the film, while Mg-3Li already shows a release similar to

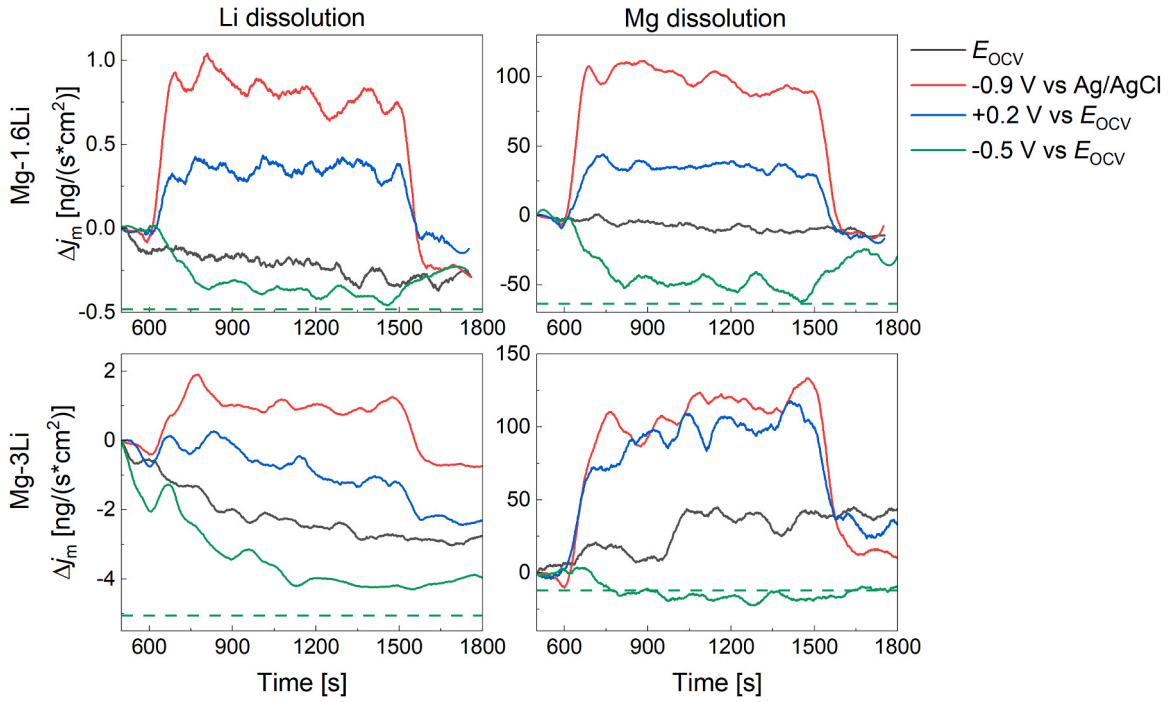

Fig. 4. Change of dissolution rate (Δj_m) of Li (a,c) and Mg (b,d), measured for Mg-1.6Li (a,b) and Mg-3Li (c,d) while holding the samples at constant voltages (E_{OCV} (Mg-1.6Li: −1.77 V, Mg3Li: −1.94 V vs. Ag/AgCl), E_{OCV} +0.2 V (Mg-1.6Li: −1.74 V, Mg3Li: −1.72 V vs. Ag/AgCl), E_{OCV} −0.5 V (Mg-1.6Li: −2.23 V, Mg3Li: −2.39 V vs. Ag/AgCl), −0.9 V vs. Ag/AgCL reference electrode) for 15 min after 10 min E_{OCV} measurement. The change is defined as the difference to the dissolution rate at E_{OCV} after 500 s. Additionally, the dashed line marks the dissolution rate change to reach a total dissolution rate j_m=0 ng/(s*cm^2) for a voltage of E_{OCV}-0.5 V to identify if the dissolution is completely suppressed.

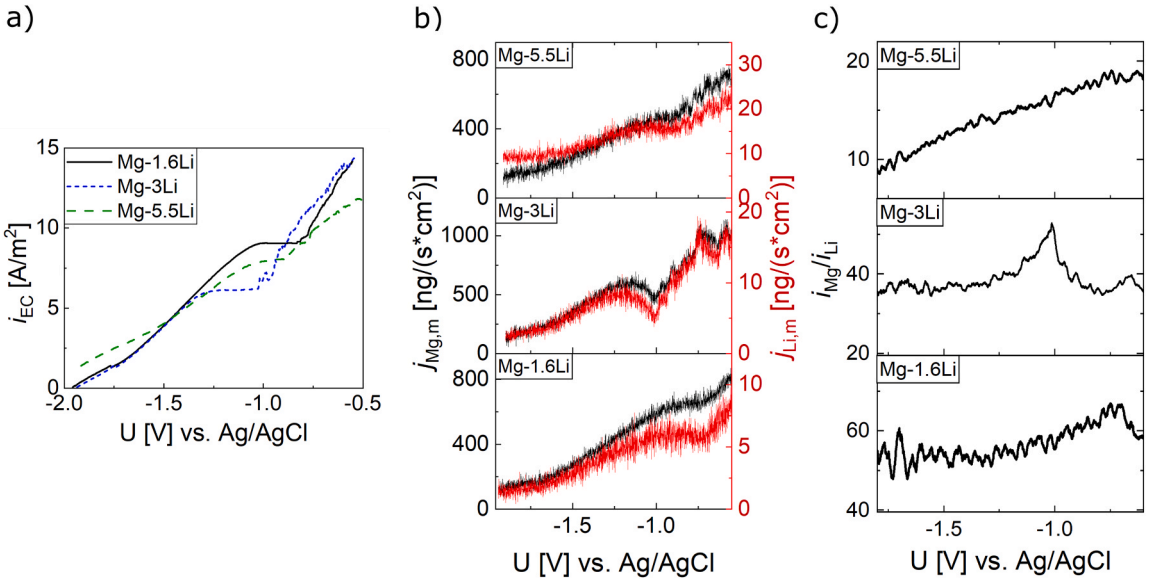

Fig. 5. LSV from E_{OCV} to −0.5 V vs. Ag/AgCl of Mg-1.6Li, Mg-3Li and Mg-5.5Li thin films. a) Current density measured in a flow cell with the potentiostat. b) Dissolution rate of Mg and Li over applied voltage. c) Ratio of dissolution current density of Mg and Li calculated from dissolution rates over applied voltage.

the ratio in the sample. The preferred Li release is then visible for both alloy types from 4 h to 72 h of immersion. Thus, while the short-term in-situ measurement showed a preferred Mg release after the first peak of Li release, which is also visible in the first hour of measurement here, this changes to a preferred release of Li, possibly due to the higher activity of Li. Due to the higher availability of Li in Mg-3Li, the first preferred Mg release is shorter, and thus, after 1 h, the preferred release changed. Mg-5.5Li again shows the highest deviations but, in general, a higher Li than Mg release after the beginning with an increasing ratio due to a very high preferred Li release in the first hour, which was already shown during the short-term degradation. While the single-phase degradation is therefore driven by the overall degradation and the preferred release of the more active species is available but influenced by a Li-depleted start of corrosion, an addition of a second phase might change the behaviour to a strong release of the highly reactive second phase by galvanic coupling.

By taking into account the results of enhanced preferred Mg dissolution after a pitting potential is applied in in-situ measurements, the

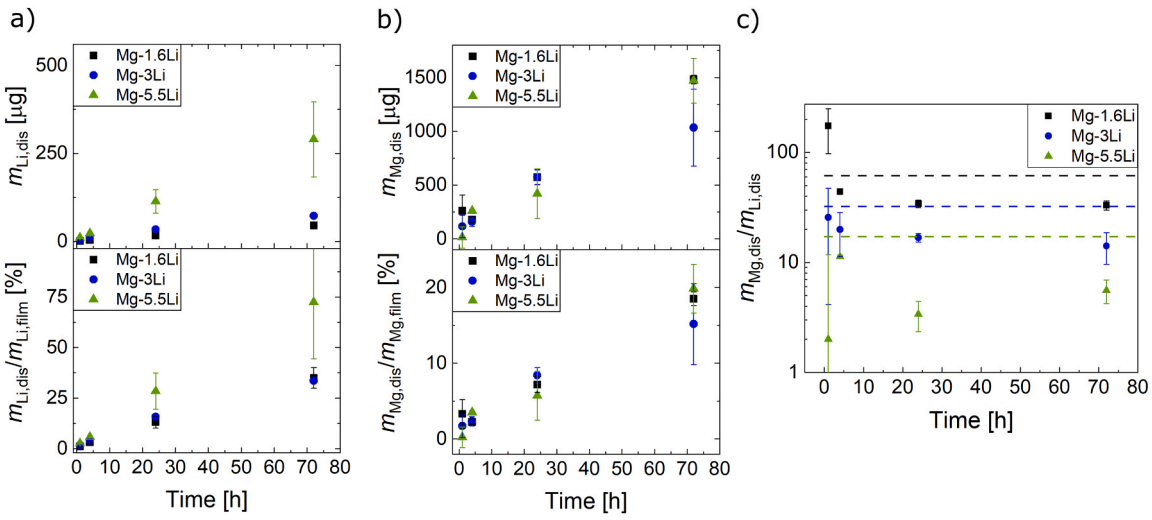

Fig. 6. 3-day ion release study in HBSS (155 mmol) at a pH of 7.4 and a temperature of 37 °C, determined by ICP-MS measurements on extracted solution. a) Total Li mass dissolved until measurement time and percentage of mass released with respect to the overall mass of Li available in the film. b) Total Mg mass released until measurement time and percentage of mass released with respect to the overall mass of Mg available in the film. c) Ratio of dissolved Mg and Li mass. The mass ratio present in the thin films (calculated from film composition) is marked with dashed lines.

change of preferred release might also be additionally influenced by a formation of corrosion products mainly containing Mg and, therefore, reducing the Mg release in comparison to Li over time.

3.3. Surface composition

As identified in the release studies, the surface composition and films

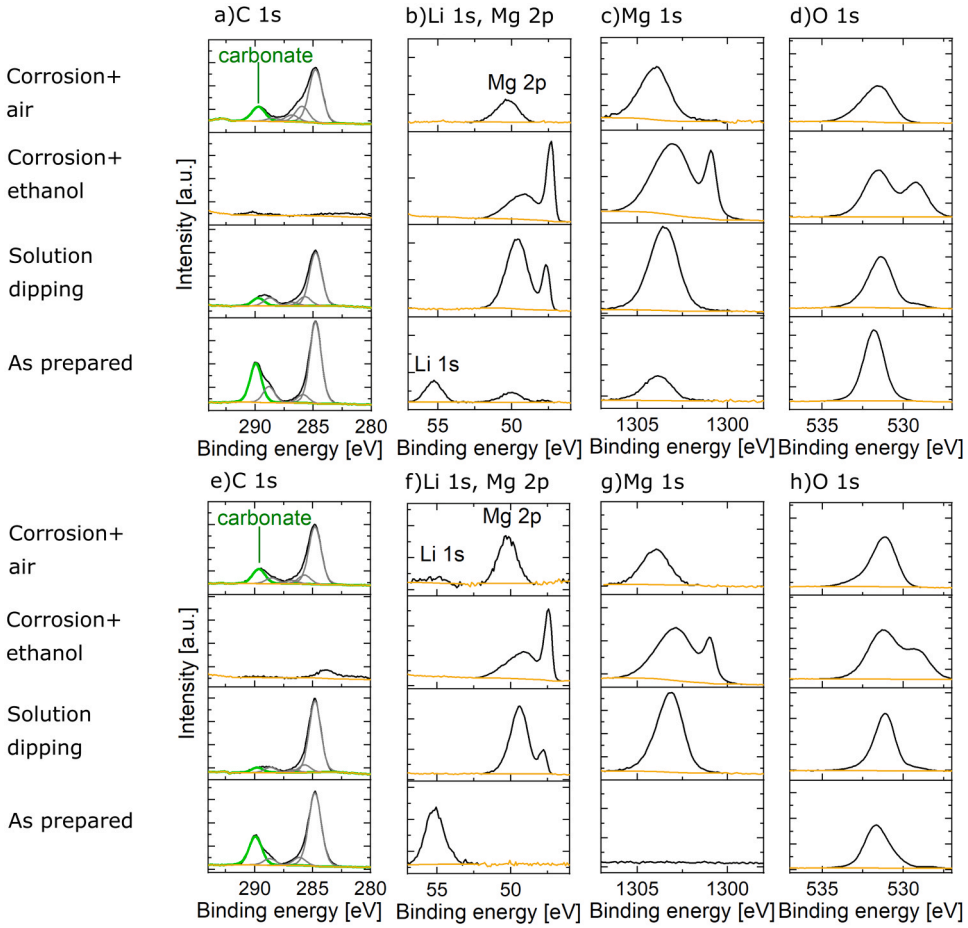

Fig. 7. XPS data of Mg-1.6Li (a-d) and Mg-3Li (e-h). a,e) C 1 s (the carbonate peal is marked on the left), b,f) Li 1 s and Mg2p, c,g) Mg 1 s, d,h) O 1 s. For each sample and measured signal, 4 samples are compared: as prepared (sputtered sample), sample dipped in solution shortly before the measurement, sample corroded for 1 h in solution and stored in air and sample corroded for 1 h in solution and stored in ethanol before measurement.

formed on as prepared and corroded samples play a significant role in the degradation process.

The surface composition is analysed by XPS on the as-prepared samples, after dipping them in solution and after corrosion for 1 h. The C 1 s, O 1 s, Mg 1 s and Li 1 s (+Mg 2p) spectra are given in Fig. 7a-d for Mg-1.6Li and Fig. 7e-h for Mg-3Li. In the as-prepared state, only for Mg-1.6Li, a Mg signal is measured on the surface. Both sample types show a strong Li 1 s peak, indicating an accumulation of Li-rich phases on the surface. The C 1 s signal also shows a carbonate peak in the as-sputtered state. For Mg-1.6Li, mainly one sharp peak (mainly hydroxide) is found in the O 1 s spectrum, while for Mg-3Li, an additional shoulder at lower binding energies indicates the presence of oxides.

The effect of contact with solution on the surface composition is studied by dipping a sample into the solution shortly before measurement. After the first contact with the solution, the Li signal disappears for both sample types while a Mg peak is now identified for both samples. Together with the sharp release of Li at the beginning of the in-situ measurements, this leads to the assumption that a Li-rich layer exists on the surface before the immersion, which makes the Li ions readily available for dissolution. The layer is thicker or more complete for films with higher Li fraction, enhancing the Li and reducing the Mg signal of Mg-3Li in comparison to Mg-1.6Li. Thus, first contact with the solution leads to a decrease of Li and carbonate content on the surface, leading to the assumption of a Li_2CO_3 layer present before, which is water soluble.

Measurements on samples corroded for 1 h in solution are carried out after storing the sample in ethanol or air for transport. As shown in Fig. 7, this influences the sample surface significantly. A strong Mg peak is still present for samples stored in ethanol to prevent contact with air, and no strong Li accumulations occur on the surface. In addition to a broadened Mg peak, a sharp additional peak (Mg-1.6Li, Mg-3Li) of Mg metal is found, thus, the oxide/hydroxide layer on the surface is thinner than 5 nm. The O 1 s signal consists of two prominent peaks at around 531.5 eV and 529 eV. While the peak at higher energy is present already on the as-prepared samples, the peak at lower energy is shown especially for Mg-3Li as a more minor shoulder after dipping the sample in solution; therefore, it is not only a signal influenced by ethanol storage. The C signal for all sample types is strongly reduced. Storing the samples in air leads to a C 1 s and O 1 s signal similar to the as prepared samples. The O 1 s signal also slightly broadened with a shoulder at higher energies, indicating the presence of carbonates. For Mg-3Li, a Li peak and carbonate can be detected. In comparison, Mg-1.6Li samples do not show any Li signal with a slight reduction and broadening in the Mg peak. Thus, the Li compound containing surface layer is formed after corrosion and contact in air, but the formation speed is dependent on the Li available for the formation since Li is present close to the surface and less diffusion is necessary for the formation.

Thus, contact with solution and corrosion does not increase the Li and carbonate content on the surface during the corrosion time of 1 h of the thin films, but contact with air does for hcp Mg-Li alloys.

Additional elements in corrosion products, such as Ca and P, can be detected on the corroded samples (stored in ethanol) (Fig. 3 supplementary). The presence of Ca and phosphates is discussed to reduce the corrosion of Mg alloys, also with additional carbonates, in a medium with added salts to simulate physiological conditions [47].

4. Discussion

4.1. Surface in air

In general, for Mg materials, a layer of MgO which partially reacts to $Mg(OH)_2$ is formed in air [27]. Yan et al. propose for Mg-Li alloys that the $Mg(OH)_2$ can react further to Mg carbonate containing compounds if stored in air, which leads to a reduction in $Mg(OH)_2$ [48]. However, for the samples in this study, the Mg signal in general is reduced and completely absent for Mg-3Li, thus, another compound is attributing to the surface composition. High Li and carbonate signals were found on the sample surface. Therefore, the formation of a Li and carbonate-containing layer is found on all sample types with a thicker or more complete layer for Mg-3Li. Li_2CO_3 is a common component formed in air on Mg-Li alloys with high Li concentration and β-phase [42,49]. For high Li concentrations, a large amount of Li is available close to the surface and can readily react. Additionally, further Li can be transported to the surface, leading to a Li-depleted zone under the surface layer [49]. However, since the PBR (Pilling-Bedworth ratio) is between 1 and 2 for all Li fractions, it can also form stably on all α-Mg-Li [26]. To support this assumption, it should be noted that Xiang et al. also found Li_2CO_3 films on a Mg-5Li-1Al hcp alloy [30].

The occurrence of a surface layer consisting mainly of Li components is also proven in the in-situ release studies by the sharp release of Li at the beginning of immersion. The peak height increases from Mg-1.6Li<Mg-3Li <Mg-5.5Li, indicating a higher amount of Li components formed when the Li content is increased, which is not necessarily dependent on the phase. Since Li_2CO_3 is water soluble [42], the layer dissolves and, therefore, does not influence the corrosion resistance of both Mg-1.6Li and Mg-3Li. The dissolution is also proven by the disappearance of the Li signal in XPS after a first short immersion. Even though it can be theoretically formed in solution, this highly depends on the availability of Li ions and carbonate and the pH [50]. Here, the measurements were performed at a pH of around 7.4, while Li_2CO_3 is more stable for alkaline solutions. The diffusion of Li to the surface can then lead to a Li-depleted, Mg-rich area underneath the surface layer, which also adds to the strong Mg signal detected by XPS after the short-term immersion.

After corrosion, samples were stored again for approximately 7 days in air. Since, for both alloys, the samples stored in ethanol after corrosion showed no Li and low carbonate signal, the change can be attributed to the exposure to air. Yan et al. found that exposure to air after corrosion leads to the formation of Li_2CO_3 on the sample surface of a bcc Mg-Li-based alloy after 60 h [48] and starts already after less than 3 hours [42]. The thickness of the Li_2CO_3 films on Mg-Li will further grow over time since more Li is transported to the surface [48]. The formation, however, is not limited to β-phase materials. While the Li diffusion coefficient in hcp Mg is lower than in β-Mg-Li [51,52], Li is still available close to the surface and can react with CO_2 from the air. Additionally, it was found that Li segregates at grain boundaries for Mg-Li alloys, also for hcp Mg-Li [53], therefore enabling fast transport due to grain boundary diffusion. Since the columnar growth or long grains for both Mg-1.6Li and Mg-3Li offer many grain boundaries and sometimes void formation [8] leading to the film surface, this can further facilitate the transport. The amount of Li available is then influenced by the Li fraction in the film. Mg-3Li presents a Li and carbonate signal on the surface after corrosion and storage in air, even though the Li signal is very low. Therefore, the formation depends on the Li content present in the hcp Mg-Li due to the higher availability close to the surface. It can be assumed that this not only increases the layer thickness as discussed for the as-prepared samples but also the speed of a detectable layer; thus, the formation of such a layer on corroded Mg-1.6Li samples after longer storage time might be possible.

4.2. Ion release and degradation

The ion release due to the degradation of the Mg-Li thin films was tested directly after the immersion in-situ and over longer time. The degradation can change over time due to the release and depletion of one element or the further prevention of fast corrosion due to corrosion products forming protective layers on the surface. For single-phase hcp Mg-Li, a corrosion similar to Mg is expected. For Mg, a thin, dense layer of MgO and a thicker, porous layer of $Mg(OH)_2$ is formed on the surface, which is more stable in an alkaline solution [50]. The pH close to the surface increases during the corrosion, stabilising such layers. The corrosion is driven by filiform corrosion with a cathodic corrosion front [26]. By adding Li, in general, the hydrogen evolution effect of Mg alloys

decreases and even though the passivation is not strong, additional compounds such as Li_2CO_3 or LiOH have been found on the surface of Mg-Li based samples [29,30].

In general, the Li release is expected to increase with the Li content available in the film, which was found for both short-term and long-term measurements. However, the release is influenced by not only the Li content but also the degradation process, in the simplest case, the corrosion rate. In a previous study, the corrosion rate of Mg-1.6Li was determined to be the lowest, while the corrosion rate increased due to the change in orientation, higher activity of Li and galvanic coupling because of the formation of a second phase for Mg-5.5Li [8]. A higher Li content leads to a higher corrosion rate and, thus, to a higher release in both Mg and Li ions. This can be even more pronounced if the increase in Li content also changes the orientation of the material and the microstructure [8]. This is in agreement with the higher overall ion release and, thus, corrosion rate measured herein.

Both α-Mg-Li alloys show a preferred Mg release after the first peak of Li release in the first hour, and there is a nearly direct start of Mg release after immersion. Thus, after the dissolution of Li-rich compounds, Li is no longer released preferentially, and a larger amount of Mg is available, possibly due to the depletion after Li reacting on the surface. In the 3-day measurements, both α-phase materials show a similar trend of release with a higher release of Mg at the beginning, as already mentioned for in-situ measurements. However, the results show a preferred dissolution of Li over longer immersion times, possibly due to the lower electrochemical potential [50]. The preferred dissolution of Li is also observed in the ion release studies at constant voltage. While the Mg release is nearly completely suppressed for both materials at cathodic polarisation, Li release still occurs, especially for Mg-3Li. Thus, the release is not a continuous release of both materials present in the phase but preferred of one material even though no two different phases can be found. Since the Li was found to be accumulating at the grain boundaries [53], it is possible that these Li-rich areas are corroding preferentially; however, further studies would be needed to prove the effect on the ion release directly.

The corrosion of α-Mg-Li, thus, changes from surface to bulk of the thin films and can be described by three phases (Fig. 8): 1. Li release from Li containing surface film formed in air, 2. Preferred release of Mg from Mg-rich area under the surface, 3. Continuous release from the bulk of the film with preferred Li dissolution. The release of Mg is reduced over time while the Li release is less reduced; thus, in addition to the higher activity of Li, the incorporation of Mg in corrosion products might additionally reduce the Mg release and lead to a higher concentration of Li in comparison to Mg. The anodic polarisation by sweeping to values above passivation and the start of pitting shows an increase of Mg release, thus indicating the presence of a Mg-rich corrosion product. The formation of the corrosion products can then change decrease corrosion over time [54] together with additional components such as phosphates (Ca, P) formed due to the additional salts in the solution. Li-containing components have not been found in the outer layer after corrosion without storage in air, and after 1 h of immersion, only a thin layer of oxides and hydroxides is formed. Thus, the Mg metal underneath is still detectable. Further measurements would be necessary to identify the composition of the corrosion products in detail which is not

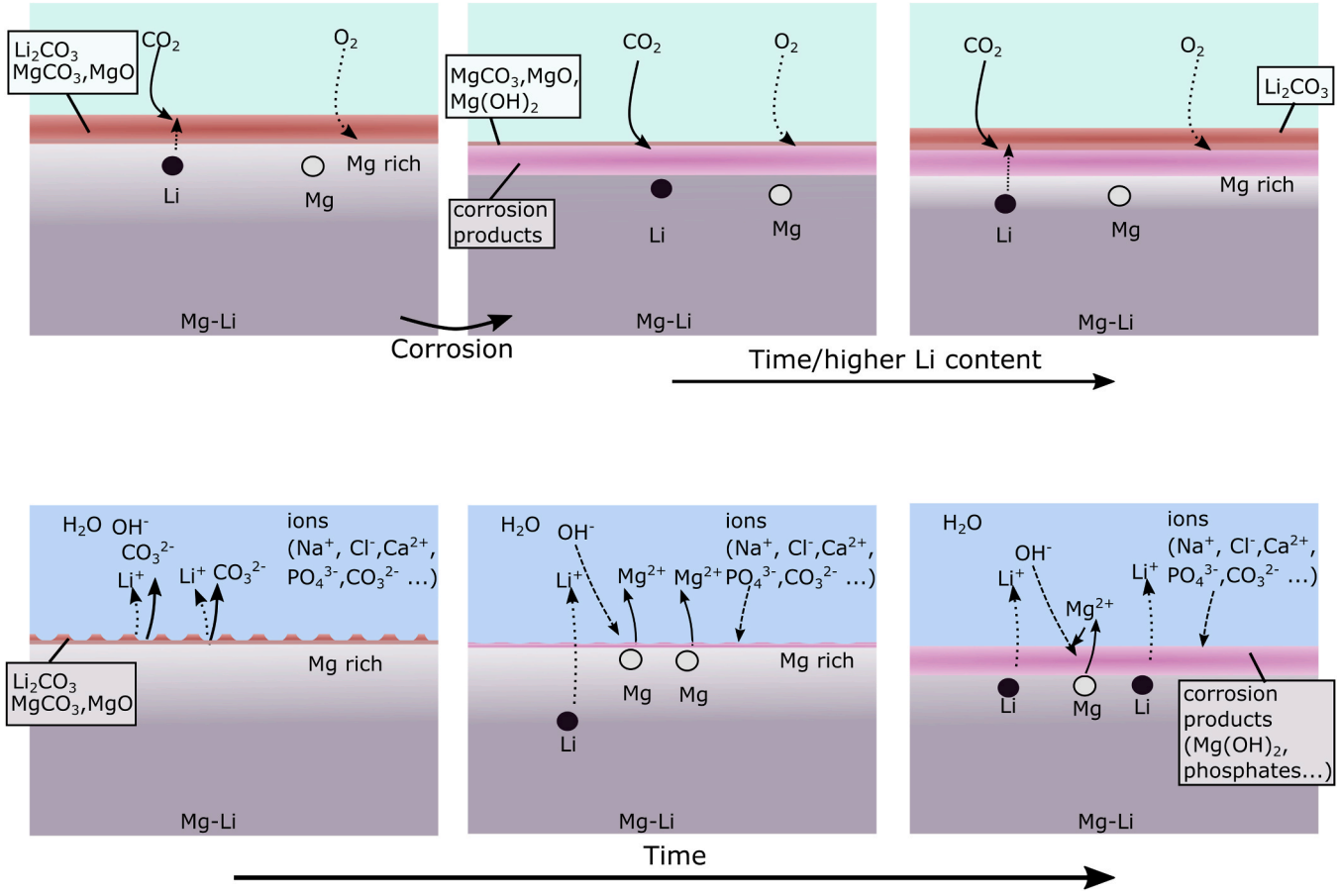

Fig. 8. Schematics of possible processes of the surface layer formation and degradation of hcp Mg-Li thin films a)-c) in air and d)-f) in solution. a) Formation of a Li_2CO_3 and MgO containing surface layer in air on as sputtered samples, b) formation of Mg-rich surface layers in air after short storage time and low Li content after corrosion and c) development of Li_2CO_3 on corroded samples after longer storage time in air for films with higher Li content. d) The start of the contact with solution leads to a dissolution of the Li-rich carbonate layer, followed by e) preferred, strong Mg release in short-term corrosion, before f) the release switches to preferred Li release, possibly due to preferred Li release and formation of corrosion products.

part of this study.

For the application of such films, the Li release needs to be determined over time. While the therapeutic range is discussed to be around 0.4–1.2 mM [55], this cannot be directly compared to the concentrations reached in the 3-day studies due to the influence of cells or placement *in vivo* on the corrosion rate [56], and the actual volume of solution and the flow on the final concentration. However, this study and the preferred release of Li identify that the Li concentration available cannot be directly derived from the degradation rate of the films and will change, especially during the beginning of placement and after long immersion times when Li is depleted. Especially the first Li-rich layer might lead to higher Li concentrations, and removal of such layer by, e.g., previous immersion in solution might be necessary.

5. Conclusions

Mg-Li thin films in the hcp phase were studied with respect to the surface chemistry and degradation by a combination of in-situ and ex-situ techniques for determining the ion release and additional analysis of the surface composition by XPS. A process of the formation of surface layers in air and during corrosion and preferred ion release is described:

- It was found that both sputtered hcp alloys (Mg-1.6Li and Mg-3Li) formed Li carbonate containing compounds on the surface after long-term exposure to air. This layer is also formed if corroded samples are exposed to air. However, the development is mainly visible for Mg-3Li films after 7 days due to the higher Li content and, thus, availability of the element.
- During degradation in Hanks' balanced salt solution, this surface layer is dissolved, monitored by a high release in Li and reduction in both carbonate and Li signal in XPS. The layer does, therefore, not contribute to the passivity and influence on the corrosion resistance of the hcp thin films.
- While a higher Mg concentration can be found during the first hour of immersion, a higher Li concentration than present in the film is determined over a longer time due to the preferred release of Li and the formation of Mg-rich corrosion products (containing oxides and hydroxides), which form a passivating layer and decrease the corrosion rate.

The corrosion process and ion release are time-dependent and change from direct contact in solution to long-term corrosion. The combination of in-situ short-term and studies with longer immersion times, as described in this work, is therefore beneficial to gain a more comprehensive picture of the complex degradation behaviour of the thin films.

Understanding the degradation process and reactions in air is also of interest for other applications of MgLi in fields such as lightweight construction. For the medical field specifically, the ion release results also highlight the importance of carefully analysing the ion release when discussing such thin films for application as biodegradable reservoirs for treatments with dissolving elements. For an optimisation of the treatment, it is not sufficient to determine the Li release by degradation rate since a change over time occurs. The change in the ratio of both ions must also be considered if both can influence the therapeutic effect of the other element involved. Furthermore, a treatment or solution dipping before tests *in vitro* or *in vivo* might be beneficial to avoid the impact of the high Li release at the start.

CRediT authorship contribution statement

Ulrike Westernströer: Investigation. **Dieter Garbe-Schönberg:** Supervision, Resources. **Lisa Hanke:** Writing – review & editing, Writing – original draft, Investigation, Formal analysis, Conceptualization. **Lukas Kalchgruber:** Writing – review & editing, Methodology, Investigation. **Eckhard Quandt:** Writing – review & editing, Supervision, Funding acquisition. **Markus Valtiner:** Writing – review & editing, Supervision, Resources, Methodology.

Declaration of Competing Interest

The authors declare that they have no known competing financial interests or personal relationships that could have appeared to influence the work reported in this paper.

Data Availability

Data will be made available on request.

Acknowledgements

This work was supported by the DFG in the framework of the research training group 2154 – Materials for Brain (project 270394294). We also acknowledge the CzechNanoLab project LM2018110 funded by MEYS CR for the financial support of the XPS measurements at CEITEC Nano Research Infrastructure.

Appendix A. Supporting information

Supplementary data associated with this article can be found in the online version at doi:10.1016/j.corsci.2024.112361.

References

[1] J.-W. Lee, H.-S. Han, K.-J. Han, J. Park, H. Jeon, M.-R. Ok, H.-K. Seok, J.-P. Ahn, K. E. Lee, D.-H. Lee, S.-J. Yang, S.-Y. Cho, P.-R. Cha, H. Kwon, T.-H. Nam, J.H.L. Han, H.-J. Rho, K.-S. Lee, Y.-C. Kim, D. Mantovani, Long-term clinical study and multiscale analysis of in vivo biodegradation mechanism of Mg alloy, Proc. Natl. Acad. Sci. U. S. A. 113 (2016) 716–721, https://doi.org/10.1073/pnas.1518238113.

[2] V. Tsakiris, C. Tardei, F.M. Clicinschi, Biodegradable Mg alloys for orthopedic implants – a review, J. Magnes. Alloy. 9 (2021) 1884–1905, https://doi.org/10.1016/j.jma.2021.06.024.

[3] G. Uppal, A. Thakur, A. Chauhan, S. Bala, Magnesium based implants for functional bone tissue regeneration – A review, J. Magnes. Alloy. 10 (2022) 356–386, https://doi.org/10.1016/j.jma.2021.08.017.

[4] S. Zaatreh, D. Haffner, M. Strauß, K. Wegner, M. Warkentin, C. Lurtz, C. Zamponi, W. Mittelmeier, B. Kreikemeyer, R. Willumeit-Römer, E. Quandt, R. Bader, Fast corroding, thin magnesium coating displays antibacterial effects and low cytotoxicity, Biofouling 33 (2017) 294–305, https://doi.org/10.1080/08927014.2017.1303832.

[5] A. Atrens, M. Liu, N.I. Zainal Abidin, Corrosion mechanism applicable to biodegradable magnesium implants, Mater. Sci. Eng. B 176 (2011) 1609–1636, https://doi.org/10.1016/j.mseb.2010.12.017.

[6] X. Li, X. Liu, S. Wu, K.W.K. Yeung, Y. Zheng, P.K. Chu, Design of magnesium alloys with controllable degradation for biomedical implants: from bulk to surface, Acta Biomater. 45 (2016) 2–30, https://doi.org/10.1016/j.actbio.2016.09.005.

[7] L. Wei, Z. Gao, Recent research advances on corrosion mechanism and protection, and novel coating materials of magnesium alloys: a review, RSC Adv. 13 (2023) 8427–8463, https://doi.org/10.1039/D2RA07829E.

[8] L. Hanke, L.K. Jessen, F. Weisheit, K. Bhat, U. Westernströer, D. Garbe-Schönberg, R. Willumeit-Römer, E. Quandt, Structural characterisation and degradation of Mg-Li thin films for biodegradable implants, Sci. Rep. 13 (2023) 12572, https://doi.org/10.1038/s41598-023-39493-9.

[9] Y. Sun, H. Zhang, Y. Zhang, Z. Liu, D. He, W. Xu, S. Li, C. Zhang, Z. Zhang, Li–Mg–Si bioceramics provide a dynamic immuno-modulatory and repair-supportive microenvironment for peripheral nerve regeneration, Bioact. Mater. 28 (2023) 227–242, https://doi.org/10.1016/j.bioactmat.2023.05.013.

[10] L. Li, X. Peng, Y. Qin, R. Wang, J. Tang, X. Cui, T. Wang, W. Liu, H. Pan, B. Li, Acceleration of bone regeneration by activating Wnt/β-catenin signalling pathway via lithium released from lithium chloride/calcium phosphate cement in osteoporosis, Sci. Rep. 7 (2017) 45204, https://doi.org/10.1038/srep45204.

[11] F. He, X. Yuan, T. Lu, Y. Wang, S. Feng, X. Shi, L. Wang, J. Ye, H. Yang, Preparation and characterization of novel lithium magnesium phosphate bioceramic scaffolds facilitating bone generation, J. Mater. Chem. B 10 (2022) 4040–4047, https://doi.org/10.1039/D2TB00471B.

[12] A.E. Kocman, I. Dag, T. Sengel, E. Soztutar, M. Canbek, The effect of lithium and lithium-loaded hyaluronic acid hydrogel applications on nerve regeneration and recovery of motor functions in peripheral nerve injury, Rend. Lince-.-. Sci. Fis. E Nat. 31 (2020) 889–904, https://doi.org/10.1007/s12210-020-00919-5.

[13] K. Bhat, L. Schlotterose, L. Hanke, H. Helmholz, E. Quandt, K. Hattermann, R. Willumeit-Römer, Magnesium-lithium thin films for neurological applications–An *in vitro* investigation of glial cytocompatibility and

neuroinflammatory response, Acta Biomater. 178 (2024) 307–319, https://doi.org/10.1016/j.actbio.2024.02.018.
[14] A. Vallée, J.-N. Vallée, Y. Lecarpentier, Parkinson's disease: potential actions of lithium by targeting the WNT/β-catenin pathway, oxidative stress, inflammation and glutamatergic pathway, Cells 10 (2021) 230, https://doi.org/10.3390/cells10020230.
[15] A. Can, T.G. Schulze, T.D. Gould, Molecular actions and clinical pharmacogenetics of lithium therapy, Pharmacol. Biochem. Behav. 123 (2014) 3–16, https://doi.org/10.1016/j.pbb.2014.02.004.
[16] C. Volkmann, T. Bschor, S. Köhler, Lithium treatment over the lifespan in bipolar disorders, Front. Psychiatry 11 (2020) 377, https://doi.org/10.3389/fpsyt.2020.00377.
[17] O.V. Forlenza, V.J.R. De-Paula, B.S.O. Diniz, Neuroprotective effects of lithium: implications for the treatment of Alzheimer's disease and related neurodegenerative disorders, ACS Chem. Neurosci. 5 (2014) 443–450, https://doi.org/10.1021/cn5000309.
[18] M. Gitlin, Lithium side effects and toxicity: prevalence and management strategies, Int. J. Bipolar Disord. 4 (2016) 27, https://doi.org/10.1186/s40345-016-0068-y.
[19] J.A.M. Maier, L. Locatelli, G. Fedele, A. Cazzaniga, A. Mazur, Magnesium and the brain: a focus on neuroinflammation and neurodegeneration, Int. J. Mol. Sci. 24 (2023) 223, https://doi.org/10.3390/ijms24010223.
[20] A.E. Kirkland, G.L. Sarlo, K.F. Holton, The role of magnesium in neurological disorders, Nutrients 10 (2018) 730, https://doi.org/10.3390/nu10060730.
[21] C. Xu, S. Wang, H. Wang, K. Liu, S. Zhang, B. Chen, H. Liu, F. Tong, F. Peng, Y. Tu, Y. Li, Magnesium-based micromotors as hydrogen generators for precise rheumatoid arthritis therapy, Nano Lett. 21 (2021) 1982–1991, https://doi.org/10.1021/acs.nanolett.0c04438.
[22] T.A. Ranathunge, D.G.G.P. Karunaratne, R.M.G. Rajapakse, D.L. Watkins, Doxorubicin loaded magnesium oxide nanoflakes as pH dependent carriers for simultaneous treatment of cancer and hypomagnesemia, Nanomaterials 9 (2019) 208, https://doi.org/10.3390/nano9020208.
[23] A. Nyabadza, C. Shan, R. Murphy, M. Vazquez, D. Brabazon, Laser-synthesised magnesium nanoparticles for amino acid and enzyme immobilisation, OpenNano 11 (2023) 100133, https://doi.org/10.1016/j.onano.2023.100133.
[24] W. Zhou, Y. Zhang, S. Meng, C. Xing, M. Ma, Z. Liu, C. Yang, T. Kong, Micro-/nano-structures on biodegradable magnesium@PLGA and their cytotoxicity, photothermal, and anti-tumor effects, Small Methods 5 (2021) 2000920, https://doi.org/10.1002/smtd.202000920.
[25] L. Dong, X. Liu, J. Liang, C. Li, Y. Dong, Z. Zhang, Corrosion behavior of a eutectic Mg–8Li alloy in NaCl solution, Electrochem. Commun. 129 (2021) 107087, https://doi.org/10.1016/j.elecom.2021.107087.
[26] C.Q. Li, D.K. Xu, X.-B. Chen, B.J. Wang, R.Z. Wu, E.H. Han, N. Birbilis, Composition and microstructure dependent corrosion behaviour of Mg-Li alloys, Electrochim. Acta 260 (2018) 55–64, https://doi.org/10.1016/j.electacta.2017.11.091.
[27] M. Taheri, M. Danaie, J.R. Kish, TEM examination of the film formed on corroding Mg prior to breakdown, J. Electrochem. Soc. 161 (2013) C89–C94, https://doi.org/10.1149/2.017403jes.
[28] B.-J. Wang, J.-Y. Luan, D.-K. Xu, J. Sun, C.-Q. Li, E.-H. Han, Research progress on the corrosion behavior of magnesium–lithium-based alloys: a review, Acta Metall. Sin. Engl. Lett. 32 (2019) 1–9, https://doi.org/10.1007/s40195-018-0847-9.
[29] C. Li, Y. He, H. Huang, Effect of lithium content on the mechanical and corrosion behaviors of HCP binary Mg–Li alloys, J. Magnes. Alloy. 9 (2021) 569–580, https://doi.org/10.1016/j.jma.2020.02.022.
[30] Q. Xiang, B. Jiang, Y. Zhang, X. Chen, J. Song, J. Xu, L. Fang, F. Pan, Effect of rolling-induced microstructure on corrosion behaviour of an as-extruded Mg-5Li-1Al alloy sheet, Corros. Sci. 119 (2017) 14–22, https://doi.org/10.1016/j.corsci.2017.02.009.
[31] C. Blawert, V. Heitmann, N. Scharnagl, M. Störmer, J. Lutz, A. Prager-Duschke, D. Manova, S. Mändl, Different underlying corrosion mechanism for Mg bulk alloys and Mg thin films, Plasma Process. Polym. 6 (2009) S690–S694, https://doi.org/10.1002/ppap.200932405.
[32] K. Schlüter, C. Zamponi, A. Piorra, E. Quandt, Comparison of the corrosion behaviour of bulk and thin film magnesium alloys, Corros. Sci. 52 (2010) 3973–3977, https://doi.org/10.1016/j.corsci.2010.08.011.
[33] Y. Liu, Y. Wu, D. Bian, S. Gao, S. Leeflang, H. Guo, Y. Zheng, J. Zhou, Study on the Mg-Li-Zn ternary alloy system with improved mechanical properties, good degradation performance and different responses to cells, Acta Biomater. 62 (2017) 418–433, https://doi.org/10.1016/j.actbio.2017.08.021.
[34] W.R. Zhou, Y.F. Zheng, M.A. Leeflang, J. Zhou, Mechanical property, biocorrosion and in vitro biocompatibility evaluations of Mg–Li–(Al)–(RE) alloys for future cardiovascular stent application, Acta Biomater. 9 (2013) 8488–8498, https://doi.org/10.1016/j.actbio.2013.01.032.
[35] K. Ogle, Atomic emission spectroelectrochemistry: real-time rate measurements of dissolution, corrosion, and passivation, Corrosion 75 (2019) 1398–1419, https://doi.org/10.5006/3336.
[36] K. Ogle, S. Weber, Anodic dissolution of 304 stainless steel using atomic emission spectroelectrochemistry, J. Electrochem. Soc. 147 (2000) 1770–1780, https://doi.org/10.1149/1.1393433.
[37] S.O. Klemm, A.A. Topalov, C.A. Laska, K.J.J. Mayrhofer, Coupling of a high throughput microelectrochemical cell with online multielemental trace analysis by ICP-MS, Electrochem. Commun. 13 (2011) 1533–1535, https://doi.org/10.1016/j.elecom.2011.10.017.
[38] S. Lebouil, O. Gharbi, P. Volovitch, K. Ogle, Mg dissolution in phosphate and chloride electrolytes: insight into the mechanism of the negative difference effect, CORROSION 71 (2015) 234–241, https://doi.org/10.5006/1459.
[39] L. Rossrucker, A. Samaniego, J.-P. Grote, A.M. Mingers, C.A. Laska, N. Birbilis, G. S. Frankel, K.J.J. Mayrhofer, The pH dependence of magnesium dissolution and hydrogen evolution during anodic polarization, J. Electrochem. Soc. 162 (2015) C333–C339, https://doi.org/10.1149/2.0621507jes.
[40] S. Thomas, O. Gharbi, S.H. Salleh, P. Volovitch, K. Ogle, N. Birbilis, On the effect of Fe concentration on Mg dissolution and activation studied using atomic emission spectroelectrochemistry and scanning electrochemical microscopy, Electrochim. Acta 210 (2016) 271–284, https://doi.org/10.1016/j.electacta.2016.05.164.
[41] L. Rossrucker, K.J.J. Mayrhofer, G.S. Frankel, N. Birbilis, Investigating the real time dissolution of mg using online analysis by ICP-MS, J. Electrochem. Soc. 161 (2014) C115–C119, https://doi.org/10.1149/2.064403jes.
[42] Y.M. Yan, A. Maltseva, P. Zhou, X.J. Li, Z.R. Zeng, O. Gharbi, K. Ogle, M. La Haye, M. Vaudescal, M. Esmaily, N. Birbilis, P. Volovitch, On the in-situ aqueous stability of an Mg-Li-(Al-Y-Zr) alloy: role of Li, Corros. Sci. 164 (2020) 108342, https://doi.org/10.1016/j.corsci.2019.108342.
[43] L. Hou, M. Raveggi, X.-B. Chen, W. Xu, K.J. Laws, Y. Wei, M. Ferry, N. Birbilis, Investigating the passivity and dissolution of a corrosion resistant Mg-33at%Li alloy in aqueous chloride using online ICP-MS, J. Electrochem. Soc. 163 (2016) C324–C329, https://doi.org/10.1149/2.0871606jes.
[44] Y. Yan, P. Zhou, O. Gharbi, Z. Zeng, X. Chen, P. Volovitch, K. Ogle, N. Birbilis, Investigating ion release using inline ICP during in situ scratch testing of an Mg-Li (-Al-Y-Zr) alloy, Electrochem. Commun. 99 (2019) 46–50, https://doi.org/10.1016/j.elecom.2019.01.001.
[45] D. Haffner, C. Zamponi, R.Lima de Miranda, E. Quandt, Micropatterned freestanding magnetron sputtered Mg-alloy scaffolds, BioNanoMat 16 (2015) 19–22, https://doi.org/10.1515/bnm-2015-0007.
[46] D. Dworschak, C. Brunnhofer, M. Valtiner, Photocorrosion of ZnO single crystals during electrochemical water splitting, ACS Appl. Mater. Interfaces 12 (2020) 51530–51536, https://doi.org/10.1021/acsami.0c15508.
[47] D. Mei, S.V. Lamaka, J. Gonzalez, F. Feyerabend, R. Willumeit-Römer, M. L. Zheludkevich, The role of individual components of simulated body fluid on the corrosion behavior of commercially pure Mg, Corros. Sci. 147 (2019) 81–93, https://doi.org/10.1016/j.corsci.2018.11.011.
[48] Y.M. Yan, O. Gharbi, A. Maltseva, X.B. Chen, Z.R. Zeng, S.W. Xu, W.Q. Xu, P. Volovich, M. Ferry, N. Birbilis, Investigating the structure of the surface film on a corrosion resistant Mg-Li(-Al-Y-Zr) Alloy, CORROSION 75 (2019) 80–89, https://doi.org/10.5006/2995.
[49] W. Xu, N. Birbilis, G. Sha, Y. Wang, J.E. Daniels, Y. Xiao, M. Ferry, A high-specific-strength and corrosion-resistant magnesium alloy, Nat. Mater. 14 (2015) 1229–1235, https://doi.org/10.1038/nmat4435.
[50] R.J. Santucci, M.E. McMahon, J.R. Scully, Utilization of chemical stability diagrams for improved understanding of electrochemical systems: evolution of solution chemistry towards equilibrium, Npj Mater. Degrad. 2 (2018) 1, https://doi.org/10.1038/s41529-017-0021-2.
[51] W. Zhong, J.-C. Zhao, First measurement of diffusion coefficients of lithium in magnesium, Materialia 11 (2020) 100674, https://doi.org/10.1016/j.mtla.2020.100674.
[52] Y. Iwadate, M. Lassouani, F. Lantelme, M. Chemla, Electrochemical study of mass transfer in Li-Mg and Li-Mg-Al alloys, J. Appl. Electrochem. 17 (1987) 385–397, https://doi.org/10.1007/BF01023304.
[53] H. Somekawa, D. Egusa, E. Abe, Grain boundary plasticity in solid solution Mg–Li binary alloy, Mater. Sci. Eng. A 790 (2020) 139705, https://doi.org/10.1016/j.msea.2020.139705.
[54] I.B. Singh, M. Singh, S. Das, A comparative corrosion behavior of Mg, AZ31 and AZ91 alloys in 3.5% NaCl solution, J. Magnes. Alloy. 3 (2015) 142–148, https://doi.org/10.1016/j.jma.2015.02.004.
[55] W. Severus, N. Kleindienst, F. Seemüller, S. Frangou, H. Möller, W. Greil, What is the optimal serum lithium level in the long-term treatment of bipolar disorder – a review? Bipolar Disord. 10 (2008) 231–237, https://doi.org/10.1111/j.1399-5618.2007.00475.x.
[56] A.H.M. Sanchez, B.J.C. Luthringer, F. Feyerabend, R. Willumeit, Mg and Mg alloys: how comparable are in vitro and in vivo corrosion rates? A review, Acta Biomater. 13 (2015) 16–31, https://doi.org/10.1016/j.actbio.2014.11.048.